Acta Materialia 144 (2018) 60–67

Contents lists available at ScienceDirect

Acta Materialia

journal homepage: www.elsevier.com/locate/actamat

Full length article

Similar local order in disordered fluorite and aperiodic pyrochlore structures

Jacob Shamblin [a, b], Cameron L. Tracy [c], Raul I. Palomares [b], Eric C. O'Quinn [b], Rodney C. Ewing [c], Joerg Neuefeind [d], Mikhail Feygenson [d], Jason Behrens [b], Christina Trautmann [e, f], Maik Lang [b, *]

[a] Department of Physics and Astronomy, University of Tennessee, Knoxville, TN 37996, USA
[b] Department of Nuclear Engineering, University of Tennessee, Knoxville, TN 37996, USA
[c] Department of Geological Sciences, Stanford University, Stanford, CA 94305, USA
[d] Chemical and Engineering Materials Division, Spallation Neutron Source, Oak Ridge National Laboratory, Oak Ridge, TN 37831, USA
[e] GSI Helmholtzzentrum für Schwerionenforschung, 64291 Darmstadt, Germany
[f] Technische Universität Darmstadt, 64287 Darmstadt, Germany

ARTICLE INFO

Article history:
Received 8 June 2017
Received in revised form
28 September 2017
Accepted 19 October 2017
Available online 23 October 2017

ABSTRACT

A major challenge to understanding the response of materials to extreme environments (*e.g.*, nuclear fuels/waste forms and fusion materials) is to unravel the processes by which a material can incorporate atomic-scale disorder, and at the same time, remain crystalline. While it has long been known that all condensed matter, even liquids and glasses, possess short-range order, the relation between fully-ordered, disordered, and aperiodic structures over multiple length scales is not well understood. For example, when defects are introduced (*via* pressure or irradiation) into materials adopting the pyrochlore structure, these complex oxides either disorder over specific crystallographic sites, remaining crystalline, or become aperiodic. Here we present neutron total scattering results characterizing the irradiation response of two pyrochlores, one that is known to disorder ($Er_2Sn_2O_7$) and the other to amorphize ($Dy_2Sn_2O_7$) under ion irradiation. The results demonstrate that in both cases, the local pyrochlore structure is transformed into similar short range configurations that are best fit by the orthorhombic weberite structure, even though the two compositions have distinctly different structures, aperiodic *vs.* disordered-crystalline, at longer length scales. Thus, a material's resistance to amorphization may not depend primarily on local defect formation energies, but rather on the structure's compatibility with meso-scale modulations of the local order in a way that maintains long-range periodicity.

© 2017 Acta Materialia Inc. Published by Elsevier Ltd. All rights reserved.

1. Introduction

The formation, structure, and mobility of defects controls the properties of most materials and is particularly important in extreme environments where energy deposition may be high and recovery periods exceptionally rapid. Not only are such conditions unavoidable for many technological applications, (*e.g.*, nuclear waste-storage, high-powered lasers, fission/fusion reactors, and spacecraft materials) but many emergent phenomena such as metallic hydrogen [1] and high temperature superconductivity [2] are thought to be only accessible under conditions far from typical. Thus, there is general interest in gaining a more fundamental understanding of order-disorder transformations.

Ion irradiation is a powerful tool for not only assessing the radiation tolerance of materials but also for producing non-equilibrium phases that cannot otherwise be recovered [3–8]. Complex oxides adopting the pyrochlore structure (general formula $A_2B_2O_7$) are particularly interesting, as they possess exceptional chemical and structural flexibility [9,10]. Some pyrochlore compositions have a remarkable tolerance to structural degradation in extreme environments, which is largely based on a unique disordering mechanism [11–15]. The pyrochlore structure ($Fd\bar{3}m$ space group) is most commonly described as a $2 \times 2 \times 2$ superstructure of fluorite (AO_2) consisting of two ordered cation sites,

* Corresponding author.
E-mail address: mlang2@utk.edu (M. Lang).

https://doi.org/10.1016/j.actamat.2017.10.044
1359-6454/© 2017 Acta Materialia Inc. Published by Elsevier Ltd. All rights reserved.

two ordered oxygen sites and one ordered oxygen vacancy (therefore often expressed by $A_2B_2O_6O'$) [9,16]. The A-site cation (16*d*) is coordinated with 6 O (48*f*) atoms and two O' (8*b*) atoms while the B-site cation (16*c*) is surrounded by 6 O atoms and two vacancies (8*a*). Studies using low-energy (<1 MeV/u) [5,17,18] and high-energy (>1 MeV/u) [19–21] ion irradiation have shown that pyrochlore has two distinct radiation responses: (*i*) an order-disorder transformation into a defect-fluorite structure, maintaining long-range crystallinity, and (*ii*) a crystalline-to-amorphous transformation, accompanied by a complete loss of long-range order.

The tendency for some compositions to disorder, and for others to amorphize, is thought to be related to the energetics of antisite defect formation (A- and B-site cation site exchange) [7,11,22]. When the A- and B-site cations are dissimilar in size, it is energetically unfavorable for them to exchange positions. Under ion irradiation or at high-pressures, such compositions (*e.g.,* $Gd_2Ti_2O_7$) cannot energetically form the disordered fluorite phase and instead amorphize [15,19,21]. In contrast, compositions with A- and B-site cations of similar size (*e.g.,* $Gd_2Zr_2O_7$) can readily incorporate antisites, making it easier for the disordered, defect fluorite structure to form and thus maintain long-range crystallinity in extreme environments.

This order-disorder behavior has been well established experimentally [17–21,23–28] and computationally [22,24,25,29,30]. However, recent findings have shown that the local structure in disordered pyrochlore is quite distinct from the expected fluorite-like ordering. Despite an average coordination number (CN) of 7 for both cations in the disordered fluorite structure, X-ray absorption [31–33] and neutron total scattering experiments [34] have shown that the A-site CN remains larger than the B-site CN, indicating that vacancies are still preferentially localized around the B-site cation. Neutron scattering pair distribution functions (PDFs) have shown that this difference in coordination yields a short-range structure that is distinct from both the pyrochlore and disordered fluorite structures, and instead yields an orthorhombic, weberite-like configuration (*Ccmm*) [35,36]. Similar to pyrochlore, the weberite-type structure is also a superstructure of fluorite but with a smaller unit cell ($\approx 2 \times \sqrt{2} \times \sqrt{2}$ superstructure). While there are many variants of weberite-type ordering [37] the best fit was obtained with A-site cations occupying 4*b* (8-coordinated) sites, B-site cations occupying 4*a* (6-coordinated) sites and mixed occupancy of 8*g* (7-coordinated) sites. This cation disorder occurs in alternating layers that is accompanied (or perhaps facilitated) by site exchange between 48*f* oxygens and 8*a* vacancies (with respect to the pyrochlore structure) within these layers. This oxygen-vacancy site exchange results in a vacancy that is still ordered but with a symmetry distinct from that of the pyrochlore structure. A recent computational study of all possible fluorite-type ordering has shown that this weberite-type configuration and one other ordered fluorite variant have negative formation energies; whereas, special-quasi-random structures (SQS) (representative of "disordered fluorite") have positive formation energies [38]. Both the weberite-type structure, as well as the ordered fluorite variant, are consistent in the local cation-oxygen coordination described above and only differ on longer length scales. In either case, aperiodic modulations of these structures lead to fully disordered cation and oxygen sublattices when averaged over the long-range structure. Recently, Raman and electron energy loss spectroscopy have indicated that the local atomic arrangement within amorphous pyrochlore may not be fully random, as previously thought, but may instead exhibit local ordering similar to that of the disordered phase [39,40].

The recent findings of locally-ordered structural units within the disordered defect-fluorite phase suggests that the formation energy of the cation antisite defect is insufficient to fully explain the radiation responses of various pyrochlore compositions. In order to develop an improved understanding of the atomic-scale processes that govern amorphization "resistance", both the order-disorder and the crystalline-to-amorphous transformation mechanisms must be understood from a multi-scale perspective. This paper describes a neutron total scattering study on the irradiation response of two pyrochlore compositions, one of which is known to disorder ($Er_2Sn_2O_7$) and the other to amorphize ($Dy_2Sn_2O_7$) under energetic ion irradiation [18]. PDF analysis reveals striking similarities between the local order retained in the amorphous and disordered materials despite their very different long-range structures, as indicated by diffraction experiments. Thus, the ability or inability of a given pyrochlore composition to assume locally ordered structural units that form a disordered (but still crystalline) array may be a more appropriate definition of radiation resistance, as compared with the formation energies of defects.

2. Methods

2.1. Sample synthesis

Polycrystalline $Er_2Sn_2O_7$ and $Dy_2Sn_2O_7$ powders were synthesized using conventional solid state techniques. Stoichiometric ratios of binary reagents were mixed and ground using a mortar and pestle in an acetone slurry and subsequently formed into pellets using a hydraulic press. These were fired at 1200 °C for 20 h and then reground, pressed, and fired at 1400 °C. Resulting pellets were ground into a fine powder (grain size ~1 μm) and analyzed for phase purity using a Huber X-ray diffractometer.

2.2. Swift heavy ion irradiation

Irradiations with 2.2 GeV ^{197}Au ions were performed at the X0 beamline of the GSI Helmholtz Center for Heavy Ion Research in Darmstadt, Germany. The polycrystalline powders were evenly dispersed and pressed into milled cylindrical indentations (diameter: 10 mm, depth: 70 μm) in custom-made aluminum sample holders. For both compounds, the electronic energy loss per unit path length (dE/dx) was determined using the SRIM code [41], assuming a theoretical density of $\rho = 8.19$ g/cm^3 for $Er_2Sn_2O_7$ and 7.97 g/cm^3 for $Dy_2Sn_2O_7$ (Supplemental Fig. 1). To ensure that the ions deposited a nearly constant dE/dx along their penetration path, the mass of sample to be pressed into a single holder was calculated by using the theoretical density, area of the indentation on each holder, and the penetration depth at which dE/dx begins to decrease. For consistency, this effective thickness was determined by the sharp peak of the derivative of the dE/dx *vs*. penetration depth curve (not shown). The mean electronic energy loss across each sample was 47.3 ± 1 keV/nm and 46.5 ± 1.2 keV/nm for $Er_2Sn_2O_7$ and $Dy_2Sn_2O_7$, respectively. The nuclear energy loss was at least three orders of magnitude lower than the electronic energy loss and was neglected. The mass per holder was calculated to be 24.7 mg and 24.4 mg for $Er_2Sn_2O_7$ and $Dy_2Sn_2O_7$, respectively. The weighed powder samples were pressed with a hydraulic press into the sample holders using a pressure of 25 MPa. This resulted in an actual sample thickness which was larger than the calculated effective thickness due to a packing density that was smaller than the theoretical density (estimated density on the order of 60% of theoretical density). However, this does not affect the dE/dx profile within the sample as the energy is only deposited within grains and not in the porous space between them.

A total of four sample holders was required to obtain sufficient sample mass for neutron scattering experiments. The four aluminum sample holders containing the pressed powders were affixed with double-sided tape to a 5 cm × 5 cm aluminum plate. To

protect against sample loss during irradiation, the entire plate was covered with a 7-μm thin aluminum foil. According to SRIM calculations, the Al foil slightly reduced the energy of the ions from 2.2 to 2.1 GeV. For each compound, all four holders were simultaneously irradiated to a fluence of 8×10^{12} ions/cm^2. The beam flux was limited to 1×10^9 ions/s·cm^2 to avoid sample heating. An unirradiated reference sample of similar mass was also prepared for neutron characterization. Following irradiation at room temperature, all pressed sample platelets were removed from the sample holders using a blunt needle and subsequently re-ground into fine powders. For each pyrochlore composition, the contents of the four holders were loaded into a quartz capillary with an outer diameter of 2 mm and a wall-thickness of 0.1 mm.

2.3. Neutron total scattering measurements

Neutron total scattering characterization was performed at the Nanoscale Ordered Materials Diffractometer (NOMAD) beamline at the Spallation Neutron Source at Oak Ridge National Laboratory [42]. Measurements were performed at room temperature with neutron exposure times of 100 and 140 min for $Er_2Sn_2O_7$ and $Dy_2Sn_2O_7$, respectively. The latter sample was measured for a longer time to account for the relatively large neutron absorption by Dy atoms. The pair distribution function, G(r), was obtained using the Fourier transform:

$$G(r) = \int_{Q_{min}}^{Q_{max}} Q(S(Q) - 1)\sin(Qr)dQ \quad (1)$$

where $S(Q)$ is the total scattering structure function and Q is the momentum transfer. Values of 0.2 Å^{-1} and 31.4 Å^{-1} were used for Q_{min} and Q_{max}, respectively.

Small-box refinement was performed using PDFgui [43]. Because modeling PDFs with two phases is complex, the number of refined parameters for each phase was minimized by only including isotropic atomic displacement parameters (ADPs). The pyrochlore phase ($Fd\bar{3}m$ space group) was refined using 8 total parameters. These included the unit cell parameter ($a = b = c$), the scale factor, the correlated motion parameter ("delta1"), the fractional "x" position for 48f oxygen sites, and 4 isotropic atomic displacement parameters (one for each Wyckoff site). The disordered fluorite phase ($Fm3m$ space group) was refined using only 5 total parameters: the unit cell parameter ($a = b = c$), the scale factor, the correlated motion parameter ("delta1"), and 2 isotropic atomic displacement parameters (one for each Wyckoff site). The weberite-type phase ($Ccmm$ space group) was refined using 17 parameters: 3 unit cell parameters ($a \neq b \neq c$), the scale factor, 8 atomic position parameters, and 5 isotropic ADPs. The position parameters included the x- and y-position for 8g sites, the x-, y-, and z-positions for 16h sites, and the x-position for all three 4c sites. Each Wyckoff site was given its own isotropic ADP (4a, 4b, and 8g cations and 16h and 4c oxygens). Although there are three unique 4c sites in the structure, these were all given the same ADP for simplicity. When approximating the amorphous phase of $Dy_2Sn_2O_7$, the weberite-type structure was also given a refinable "spdiameter" parameter which represents the diameter of the nanoparticle. "Delta1" was not refined for the nanoparticle approximation since the refined particle diameter was so small that the effects of correlated motion are not extremely important.

"Boxcar" refinements were carried out using the "r-series" macro in PDFgui. The initial fit-range was 1.5–11.5 Å. Subsequent fits were performed by increasing this 10 Å window to higher r in 1.5 Å increments (*i.e.*, 1.5–11.5 Å → 3–13 Å → 4.5–14.5 Å and so on). The initial parameters for each refinement were based on the final values of the previous fit. The correlated motion parameter was fixed at higher r windows, as it does not significantly affect the PDFs beyond a few Å.

3. Results

3.1. Long-range structure - neutron diffraction analysis

In agreement to the initial X-ray characterization, neutron diffraction revealed no evidence of impurities or preexisting disorder in the unirradiated samples. Both pyrochlores were refined with the fully ordered pyrochlore structure with a goodness-of-fit value (R_{WP}) of 10.2% for $Er_2Sn_2O_7$ and 7.07% for $Dy_2Sn_2O_7$ (Supplemental Fig. 2). Disorder is indicated in irradiated $Er_2Sn_2O_7$ (2.2 GeV Au ions to a fluence of 8×10^{12} ions/cm^2) by the reduced intensity of all diffraction maxima and the disappearance of pyrochlore superstructure peaks in the total scattering structure function, S(Q)−1 data (Fig. 1a). No amorphization is observed for this sample, as it lacks a broad, diffuse scattering peak. This yields a slight discrepancy with a previous synchrotron X-ray diffraction study of $Er_2Sn_2O_7$ also irradiated with 2.2 GeV Au ions [39]. In that study, the primary transformation was pyrochlore-to-disordered fluorite for this composition but at the same fluence a small amount of amorphization was evident. This discrepancy can be attributed to the higher resolution of the synchrotron XRD pattern, due to the higher photon flux and lower experimental background obtained when using synchrotron X-rays, making small amorphous peaks more apparent. An alternative explanation is in the variation of the ion fluence between the two independent irradiations of the previous [39] and present study. The synchrotron samples were 40-

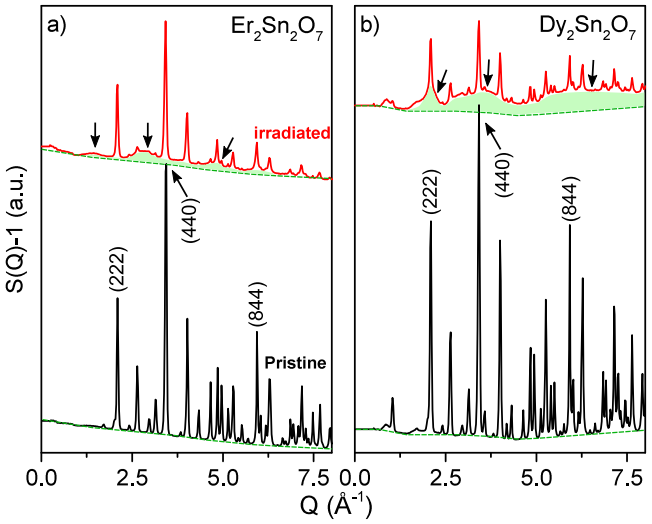

Fig. 1. Total scattering structure function, S(Q) − 1, measured by neutron scattering for pyrochlores before (black) and after (red) ion irradiation with 2.2 GeV Au ions to a fluence of 8×10^{12} ions/cm^2. (**a**) Data for $Er_2Sn_2O_7$ pyrochlore with weak diffuse scattering bands being evident in the irradiated sample (black arrows) that do not overlap with substructure Bragg peaks (Miller indices are labeled). Dashed green lines denote the "baseline" for the pristine sample which has also been offset by the same amount as the data for the irradiated sample. The green, shaded area represents diffuse scattering. (**b**) Data for $Dy_2Sn_2O_7$ pyrochlore with diffuse peaks being much more evident and overlapping with substructure Bragg reflections in the pristine sample (Miller indices are indicated). This response is similar to radiation induced amorphization observed with X-ray diffraction [39]. The baselines of the pristine S(Q)−1 are inconsistent between the two compositions due to differing neutron absorption resonances for Er and Dy and possibly water adsorbed onto the surface of the powders. (For interpretation of the references to colour in this figure legend, the reader is referred to the web version of this article.)

μm thin platelets of a few mm in diameter, while for neutron scattering experiments, samples of much larger surfaces are required. Suitable large-area irradiations were performed by magnetically defocusing the beam such that a 5 cm × 5 cm area was homogeneously irradiated. However, beam instabilities may result in fluence uncertainties of such large samples well beyond 30%. In either case, both studies are consistent in that swift heavy ion irradiation causes predominantly a transition to a disordered, long-range defect fluorite structure for this specific pyrochlore composition. Small diffuse scattering peaks are present in the neutron diffraction pattern of the irradiated sample (see arrows in Fig. 1a) which have been similarly observed in previous neutron studies on disordered pyrochlore compositions (including this composition) [36]. This diffuse scattering has been attributed to the presence of local weberite-type ordering.

$Dy_2Sn_2O_7$, irradiated under identical conditions, shows a drastically different radiation response, as indicated by the S(Q)−1 data (Fig. 1b). There is clear evidence of radiation-induced amorphization by the appearance of three broad diffuse scattering bands overlapping the (222), (440), and (844) diffraction maxima. Accompanying the growth of these amorphous bands, the diffraction peaks from the ordered pyrochlore phase are significantly reduced in intensity. The fact that pyrochlore peaks are still observable suggests that the sample has not been fully amorphized, meaning that ion tracks have not completely overlapped in the irradiated sample.

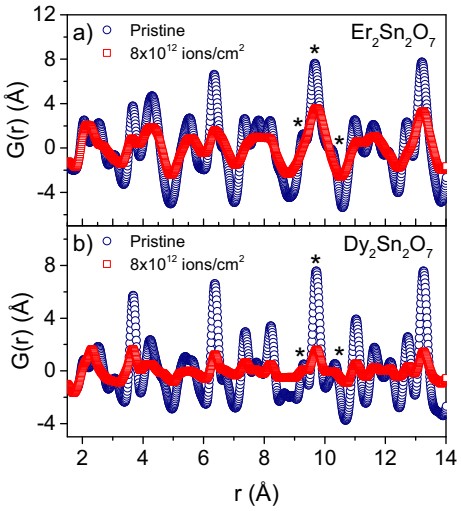

Fig. 2. Neutron PDFs (G(r)) of pyrochlores before (blue) and after (red) being irradiated with 2.2 GeV Au ions to a fluence of 8 × 10^{12} ions/cm^2. (**a**) $Er_2Sn_2O_7$, disorder is indicated by broadening and merging of the original pyrochlore peaks. (**b**) $Dy_2Sn_2O_7$, after irradiation the peaks are significantly reduced in area, but do not show pronounced merging, indicative of partial amorphization. The asterisks illustrate the irradiation behavior of three individual peaks, which either (**a**) merge into a single peak or (**b**) remain as individual peaks. (For interpretation of the references to colour in this figure legend, the reader is referred to the web version of this article.)

3.2. Short-range structure — neutron pair distribution function analysis

As with the diffraction patterns, which characterize the long-range structure, the neutron PDFs for unirradiated $Er_2Sn_2O_7$ and $Dy_2Sn_2O_7$ can be reproduced using the fully ordered pyrochlore-structure model (Supplemental Fig. 3). This implies that, prior to irradiation, there are no significant local distortions present in the as-synthesized samples and that the local structure is consistent with the long-range structure. In agreement with their distinct long-range structural responses, the PDFs for irradiated $Er_2Sn_2O_7$ (Fig. 2a) and $Dy_2Sn_2O_7$ (Fig. 2b) show significantly different structural responses at intermediate *r*-ranges (*i.e.,* radial distances beyond ≈ 5 Å, in which local polyhedra begin to repeat). Individual peaks of $Er_2Sn_2O_7$ broaden significantly in this region and convolute into single peaks after irradiation, without a large decrease in the overall peak area (see asterisks in Fig. 2a). Since PDF peak positions correspond to atom-pair separations and peak area is proportional to the number of atom-atom correlations (*i.e.*, coordination), this behavior is indicative of an order-disorder transition in which multiple crystallographic sites are degraded into fewer sites, resulting in a distribution of atomic separations within single peaks of the PDF. Small-box refinement of the PDFs over the intermediate *r*-range in irradiated $Er_2Sn_2O_7$ shows good agreement with the disordered, defect-fluorite structure model used for refining the long-range diffraction data (*e.g.,* $R_W = 10.3\%$ for $r = 9.5$–18.5 Å, Supplemental Fig. 4). Thus, the intermediate-range structural response of $Er_2Sn_2O_7$ to swift heavy ion irradiation is consistent with its long-range response.

PDF peaks in the intermediate *r*-range for irradiated $Dy_2Sn_2O_7$ show minimal broadening, but instead exhibit a significant reduction in intensity and peak area (Fig. 2b). This indicates that precise atom-atom correlations are lost over these *r*-ranges, which is consistent with the ion-induced amorphization process observed for the long-range structure by neutron diffraction (Fig. 1b). A fully amorphized sample would exhibit a PDF with no remaining peaks at large *r*-values. Small peaks evidence unirradiated and thus untransformed domains of pyrochlore, consistent with the neutron diffraction data (Fig. 1b). For example, refining from $r = 16.5$–26.5 Å using the pyrochlore-structure model yields an R_W value of 12.5% (Supplemental Fig. 5a), which is comparable to that of the unirradiated sample refined using identical parameters ($R_W = 11.1\%$, Supplemental Fig. 5b), indicating that this remaining crystallinity is well-represented by the initial pyrochlore structure. Despite reduced area at high-*r*, the peak areas at lower *r*-values remain for the most part unchanged. This is particularly evident below 3 Å, a region that corresponds to individual coordination polyhedra. In contrast to the intermediate *r*-values, atom-atom correlations are preserved in the local structure, but the changes in peak position and intensity ratios evidence a structural transition.

While the long-range (determined by S(*Q*) - 1, Fig. 1) and intermediate-range (determined by PDFs, Fig. 2) regions of the two compounds display a significantly different structural response (disordering for $Er_2Sn_2O_7$ and amorphization for $Dy_2Sn_2O_7$), both compositions reveal similar structural modifications at the local structure, particularly with regards to intra-polyhedra distances. The PDF of irradiated $Er_2Sn_2O_7$ shows that the local structure is significantly modified from the original ordered pyrochlore phase (Fig. 3a). Although there are likely remnants of pyrochlore ordering from unirradiated regions in the sample, they can no longer be discerned in the PDF of the irradiated sample. Vertical dashed lines in Fig. 3a indicate the refined atom-atom correlation positions using the pyrochlore structural model for pristine $Er_2Sn_2O_7$ (blue squares). Er is coordinated with only two O2 atoms, and the corresponding correlation peak is highly convoluted with the Sn − O1 and Er − O1 peaks (O1 refers to 48*f* oxygens). After irradiation, the Sn − O1 correlation decreases slightly while the Er − O1 correlation decreases significantly. A new atomic correlation appears at *r* values close to that of Er − O2 in the pristine pyrochlore. Since Er − O1 decreases much more significantly than Sn − O1, the new correlation could be interpreted as a shift of the Er − O1 peak to lower *r* values. This suggests that the ErO_8 scalenohedra are possibly more susceptible to distortions than SnO_6 octahedra. Similar conclusions were made from a previous Raman and X-ray absorption spectroscopy study on irradiated titanate and zirconate pyrochlores in

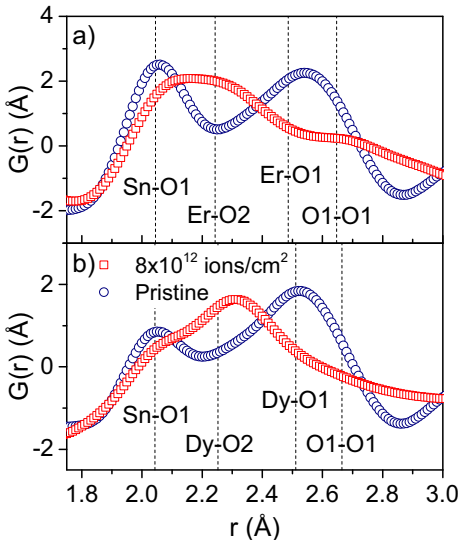

Fig. 3. Neutron PDFs in the *r*-range 1.75 to 3 Å for pristine (open blue circles) and ion irradiated (open red squares) pyrochlores. (**a**) Neutron PDFs for pristine and ion irradiated $Er_2Sn_2O_7$. (**b**) Neutron PDFs for pristine and ion irradiated $Dy_2Sn_2O_7$. Vertical dashed lines denote refined atom-pair positions in the pristine pyrochlore samples. O1 and O2 refer to 48*f* and 8*b* oxygens respectively. A qualitatively similar transformation occurs for both irradiated $Er_2Sn_2O_7$ (disordered) and $Dy_2Sn_2O_7$ (amorphized). (For interpretation of the references to colour in this figure legend, the reader is referred to the web version of this article.)

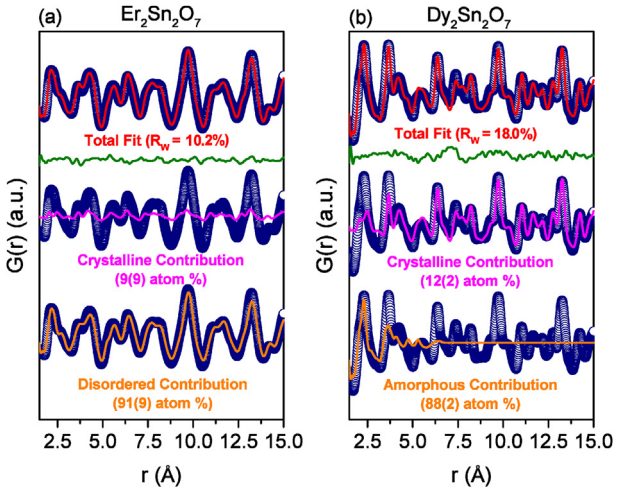

Fig. 4. Phase contributions to small-box refinements of neutron PDFs for pyrochlores irradiated with 2.2 GeV Au ions. (**a**) Experimental neutron PDF for $Er_2Sn_2O_7$ (blue circles) refined with the ordered pyrochlore (from unirradiated regions) and weberite-type (from damaged regions) structures simultaneously. The red line represents the total fit to the data using both models while the magenta and orange lines are the individual contributions corresponding to the pyrochlore and weberite models, respectively. The solid green line represents the difference between the data and the fit. (**b**) Experimental neutron PDF for $Dy_2Sn_2O_7$ (blue circles) refined with the ordered pyrochlore and nanocrystalline, weberite-type ("amorphous") structures simultaneously. The red line represents the total fit to the data using both models while the magenta and orange lines are the individual contributions coming from the pyrochlore and weberite-type model, respectively. The amorphous phase was modeled as a spherical nanoparticle with the weberite-type structure. The solid green line represents the difference between the data and the fit. (For interpretation of the references to colour in this figure legend, the reader is referred to the web version of this article.)

which the BO_6 octahedra were considered the structural "backbone" of the material [44]. It has previously been shown through small-box refinement of neutron PDFs of various "disordered fluorite" pyrochlores, including $Er_2Sn_2O_7$ used in the present study, that a *local* disordered fluorite configuration does not occur and modelling the resulting short-range structural modifications with orthorhombic weberite-type ordering over short length scales (<10 Å) instead reduces the R_w value by a factor of 2 [36].

Despite becoming amorphous over longer length scales, the short-range structure of $Dy_2Sn_2O_7$ is strikingly similar to that of $Er_2Sn_2O_7$ (Fig. 3b). The Sn − O1 and Dy − O1 peaks both decrease in similar fashion compared to the Sn − O1 and Er − O1 peaks in $Er_2Sn_2O_7$, while a new peak forms at *r*-values between these two correlations. As was the case in $Er_2Sn_2O_7$, this can be viewed as the Dy − O1 peak shifting to smaller *r*-values. The PDFs for the two samples after irradiation appear to be slightly different (*e.g.*, the new peak that forms at ≈ 2.3 Å is much stronger for $Dy_2Sn_2O_7$ compared with $Er_2Sn_2O_7$). However, this is due to the much stronger neutron scattering length for Dy atoms (16.9−2*i* and 7.79 fm for Dy and Er atoms, respectively). We have employed small-box refinement of both PDFs to test the degree of agreement between the weberite-type structure and the experimental data.

As shown in Fig. 4a, the weberite-type structure describes the short-range correlations in the neutron PDF very well for ion irradiated, disordered $Er_2Sn_2O_7$. A pyrochlore contribution to the simulated PDF was also included to account for undamaged regions within the sample (magenta curve in Fig. 4a); however, the refined weberite-type phase fraction (orange curve in Fig. 4a) was within error of a complete transformation (91(9) atom %). Small-box refinement relies on preserving periodicity which makes modeling amorphous phases rather difficult. However, the PDF for $Dy_2Sn_2O_7$ can be modelled surprisingly well by approximating the amorphous phase as a spherical weberite-type nanoparticle with a diameter of about 7 Å (orange curve in Fig. 4b). This models the material as a collection of weberite-type-ordered regions that specifically have order that does not extend beyond the length scale of the "nanoparticle" such that over longer spatial scales (*i.e.*, what is probed with diffraction) the material can be considered aperiodic. Just like an amorphous material, the area of PDF peaks of a nanocrystalline material gradually falls off at higher *r*−values as the number of atom-atom correlations decreases. The pyrochlore structure was again included to account for the undamaged regions in the sample (magenta curve in Fig. 4b). The refined fraction of the weberite-type phase was 88(2) atom %. While the modelled pyrochlore phase fractions of the PDFs are very similar for both compositions, this contribution is much more evident in $Dy_2Sn_2O_7$ because the amorphous domain has no correlations at large *r*-values, whereas it is highly convoluted with the disordered phase in $Er_2Sn_2O_7$.

Despite the good fit, in general, to the data, the refinement for $Dy_2Sn_2O_7$ is slightly inferior to that for $Er_2Sn_2O_7$ (R_W = 18.0% and 10.2%, respectively). This likely arises from the transition from the local- to intermediate-range structures. Examining the difference curve for $Dy_2Sn_2O_7$, there is a region of poor fit at approximately 7.5 Å, which is just beyond the length scale of the refined "nanoparticle" diameter (7.2(8) Å). This discrepancy between the model and the data is not surprising, as the nanoparticle approximation cannot predict indirect correlations between one weberite-ordered "unit" and another. This indicates that the amorphous phase remains weakly correlated even beyond 7.2 Å. Restricting the fit range to remain within the "nanoparticle" and thus only including direct correlations between atoms in ordered units greatly improves the fit for $Dy_2Sn_2O_7$ (*e.g.*, R_W = 11.3% for *r* = 1.5–6.5 Å). This agreement between the simulated and experimental data is excellent, demonstrating that the local atomic arrangement in the amorphous phase is indeed very similar to that of the disordered phase.

4. Discussion

Based on the comparison of neutron diffraction data with PDF results, we have shown that locally ordered structural "units", which are best fit with the orthorhombic weberite structure, exist in both the amorphous and disordered pyrochlore oxides. The existence of a locally ordered structure within both the amorphous and disordered domains was previously suggested by EELS [40] and Raman spectroscopy [39] results. While these spectroscopic studies indirectly indicated the existence of similar local order, the PDF results of the present study provide direct evidence that the local order can be described as having a weberite-type character. The only difference between amorphous and disordered pyrochlores is the amount of atomic-scale periodicity at longer length-scales.

An important aspect of the local order within irradiated pyrochlore oxides is the spatial extent of these weberite-type domains within the disordered and amorphous long-range network. This can be deduced from the neutron PDF data by adjusting the fit range over different *r*-regions (so called "boxcar refinement" [43]) and comparing the obtained goodness-of-fit values (R_W). This was completed by using the structure that best represents the PDF at large *r*-values: remnants of the pyrochlore phase from unirradiated regions in $Dy_2Sn_2O_7$ and the disordered fluorite structure in $Er_2Sn_2O_7$. Again, we stress that the $Er_2Sn_2O_7$ likely has a pyrochlore contribution at high-*r* as well (Fig. 4a), but the predominant phase contributing to the PDF is disordered fluorite. As expected, the refinement at low-*r* is very poor for both samples given the local order that is present (Fig. 5). However, as the fit-range is expanded to include correlations associated with the intermediate- and long-range structures, the R_W value initially decreases, indicating a better fit. The R_W values eventually stop decreasing and saturate with a further increase of the fit range. The *r*-value of this saturation indicates the point at which local ordering no longer has a significant contribution to the PDF and thus represents the dimension of the domains that feature this distinct short-range ordering. For "amorphous" $Dy_2Sn_2O_7$, this represents the size of the nanometric ordered domains, while in disordered $Er_2Sn_2O_7$ it represents the distance beyond which weberite-type structural units are in some way modulated to yield an average disordered-fluorite structure. Interestingly, the correlation length of the orthorhombic, weberite-type ordering appears to be very similar for both $Er_2Sn_2O_7$ and $Dy_2Sn_2O_7$ (~8 Å). This indicates that both materials consist of similarly-sized weberite-type structural units that differ only in the presence or absence of intermediate- and long-range modulated periodicity of these units.

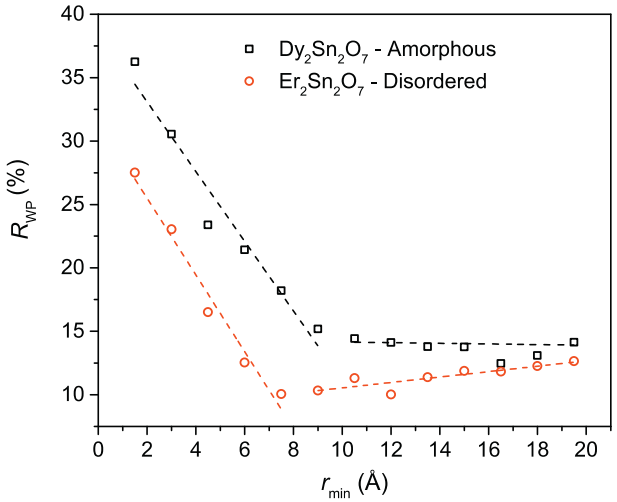

Fig. 5. Goodness-of-fit parameters (R_W) over multiple r-ranges. R_W values were obtained from refinement of neutron PDFs of $Dy_2Sn_2O_7$ (black squares) and $Er_2Sn_2O_7$ (red circles) irradiated with 2.2-GeV Au ions to a fluence of 8×10^{12} ions/cm^2. Small-box refinement was applied to both compositions using the structural model which best described the intermediate range structure (the pyrochlore phase for $Dy_2Sn_2O_7$ and the disordered fluorite phase for $Er_2Sn_2O_7$). The *x*-axis (r_{min}) represents the minimum *r*-value used for each refinement procedure while keeping the overall fit ranges to 10 Å (*e.g.*, 1.5–11.5 Å). The R_W value significantly increases below a similar fit range for both samples (9–19 Å for $Dy_2Sn_2O_7$ and 7.5–17.5 Å for $Er_2Sn_2O_7$.), which provides the spatial extend of the weberite-type ordering as the lower bound of the fit range (about 8 Å for both compositions). Dashed lines are a guide to the eye. (For interpretation of the references to colour in this figure legend, the reader is referred to the web version of this article.)

These results provide a new view of the radiation response of pyrochlore, in particular the disordering *versus* amorphization behavior. The ordered cubic structural units of the pyrochlore phase are transformed under ion irradiation (and most likely also at other extreme conditions, such as high temperatures and pressures [36]) to weberite-type orthorhombic units of very similar spatial extension (approximately 8 Å), regardless of the composition and the associated long-range structural modification. The final long-range radiation response depends then on the pyrochlore composition as to whether the local weberite-type arrangement modulates into the long-range defect-fluorite type arrangement, maintaining overall crystallinity, or into a long-range aperiodic phase. Thus, the presence of similar local order in disordered *vs.* amorphous pyrochlores (which both have high disordering energies [11,22,45]) suggests that the dominating factor determining radiation tolerance is not simply a material's ability to incorporate local disorder, but rather its ability to adopt pseudo-periodic modulations of this local order in such a way that long-range crystallinity is maintained.

Antisite defects, the formation of which is a step in the disordering of pyrochlores to an average fluorite structure, are energetically expensive when the relative sizes of the cations differ significantly [11,22,45]. MD simulations have suggested that the ratio of cation ionic radii, r_A/r_B, determines the ability of a pyrochlore material to recrystallize into the defect-fluorite structure during the rapid quenching of a "molten" volume produced during swift heavy ion irradiation-induced energy deposition [25]. The simulations showed that an amorphous ion track will form if the recrystallization rate is slower than the quench rate, and a disordered fluorite structured track will form in the opposite case. The recrystallization rate is determined by the degree of cation-size mismatch (*i.e.*, r_A/r_B). First principles calculations, however, have shown that for most stannate pyrochlores, the increased bond-covalency of Sn–O atom pairs raises the disordering energy to much larger values than would be expected simply based on r_A/r_B for more ionic B-site cations (*i.e.*, Ti and Zr) [22,30]. Thus, it has been puzzling that certain stannate pyrochlores (*e.g.*, $Y_2Sn_2O_7$ and $Er_2Sn_2O_7$) are remarkably resilient to radiation-induced amorphization [18] despite having higher disordering energies than other compositions that easily become amorphous.

Our results suggest that the recrystallization rate might not be determined *directly* by the relative size of the two cations or the disordering energy of incorporating single defects, but rather by the mobility of the weberite-type structural units that form during ion track formation. This assumes that the locally-ordered weberite units, which appear to be a universal phenomenon in pyrochlore oxides based on the present and previous work [36,38,39,46], also exist as local order within the "molten" phase. The recrystallization rate would then be determined by the mobility of locally existing polyhedral units (rather than individual atoms) and their ability to polymerize or connect to each other to form a long-range crystalline structure over femto-to picosecond time frames.

The local order in amorphous $Dy_2Sn_2O_7$ demonstrated here is

distinctly different from that predicted by a recent computational study by Xiao *et al.* on amorphization in titanate pyrochlores [47]. In that study, the local structural evolution was investigated as a function of electronic excitation concentration, as would be produced by exposure of a material to ionizing radiation. The authors found that above a certain excitation threshold, $Sm_2Ti_2O_7$, $Gd_2Ti_2O_7$, and $Y_2Ti_2O_7$ were predicted to transform to an amorphous phase within several picoseconds. Simulations revealed the formation of O_2-like molecules with an O-O separation of ~1.4 Å. The authors explained the amorphization of the cation sublattice as being driven by this O_2 formation on the oxygen sublattice. This is reflected in the modeled radial distribution function, RDF (a different variant of the PDFs used in the present study), by a new peak forming at 1.4 Å and a strong decrease in intensity in higher-*r* peaks. In the current neutron PDF analysis, the existence of predicted O_2-like molecules in irradiated $Dy_2Sn_2O_7$ is not observed, based on the behavior of the Sn-O and Dy-O correlations after irradiation. In the work of Xiao *et al.*, the formation of O_2-like molecules is accompanied by a severe decrease in all local polyhedra correlations in the modelled RDFs. Amorphous $Dy_2Sn_2O_7$ in the present study, however, exhibits retention of local order in the form of weberite-like ordering characterized by the formation of the strong peak near the original Dy-O2 correlation. The modeled RDF of $Gd_2Ti_2O_7$ does show a slight increase in coordination at the original Gd-O2 peak location, but this is not the predominant correlation within the amorphous phase as it is with irradiated $Dy_2Sn_2O_7$ in the present study (Figs. 2 and 4). However, the existence of O_2-like molecules in amorphous $Dy_2Sn_2O_7$ cannot be fully excluded due to artifacts created at very low r −values (<1.75 Å) resulting from noise in the baseline of $S(Q) - 1$ caused by strong neutron absorption from Dy atoms (Fig. 1). The simulations did predict weak correlations within the amorphous phase that extend to *r*-values of at least 7 Å, which is consistent with present results.

5. Conclusion

In conclusion, the neutron total scattering data presented in this report suggests that irradiation-induced modifications to the local structure of pyrochlore oxides are very similar for a pyrochlore composition that disorders to defect fluorite ($Er_2Sn_2O_7$) or becomes amorphous ($Dy_2Sn_2O_7$). In both cases, the local structure after irradiation can be modeled as being comprised of small regions of weberite-type, atomic-scale configurations of similar spatial extent (7–9 Å). This similarity between the disordered and aperiodic states suggests that a pyrochlore's propensity to disorder rather than to amorphize may not be fully determined by its ability to incorporate point defects, but rather by its ability to rearrange larger ordered domains that maintain long-range periodicity.

Acknowledgements

This work was supported as part of by the Materials Science of Actinides, an Energy Frontier Research Center funded by the US Department of Energy, Office of Science, Basic Energy Sciences under Award # DE-SC0001089. J.S. acknowledges support from an Organized Research Unit from the Office of Research at the University of Tennessee. This research used resources at the Spallation Neutron Source, a DOE Office of Science User Facility operated by the Oak Ridge National Laboratory. R.I.P. acknowledges support from the US Department of Energy (DOE) National Nuclear Security Administration (NNSA) through the Carnegie DOE Alliance Center (CDAC) under grant number DE-NA-0002006.

Appendix A. Supplementary data

Supplementary data related to this article can be found at https://doi.org/10.1016/j.actamat.2017.10.044.

References

[1] N.W. Ashcroft, Metallic hydrogen: a high-temperature superconductor? Phys. Rev. Lett. 21 (1968) 1748–1749.
[2] A.P. Drozdov, M.I. Eremets, I.A. Troyan, V. Ksenofontov, S.I. Shylin, Conventional superconductivity at 203 kelvin at high pressures in the sulfur hydride system, Nature 525 (7567) (2015) 73.
[3] M. Lang, F. Zhang, J. Zhang, J. Wang, B. Schuster, C. Trautmann, R. Neumann, U. Becker, R.C. Ewing, Nanoscale manipulation of the properties of solids at high pressure with relativistic heavy ions, Nat. Mater. 8 (10) (2009) 793–797.
[4] B.P. Uberuaga, M. Tang, C. Jiang, J.A. Valdez, R. Smith, Y.Q. Wang, K.E. Sickafus, Opposite correlations between cation disordering and amorphization resistance in spinels versus pyrochlores, Nat. Commun. 6 (2015).
[5] J. Lian, L.M. Wang, S.X. Wang, J. Chen, L.A. Boatner, R.C. Ewing, Nanoscale manipulation of pyrochlore: new nanocomposite ionic conductors, Phys. Rev. Lett. 87 (14) (2001).
[6] C.L. Tracy, M. Lang, F. Zhang, C. Trautmann, R.C. Ewing, Phase transformations in Ln_2O_3 materials irradiated with swift heavy ions, Phys. Rev. B 92 (17) (2015).
[7] K.E. Sickafus, R.W. Grimes, J.A. Valdez, A. Cleave, M. Tang, M. Ishimaru, S.M. Corish, C.R. Stanek, B.P. Uberuaga, Radiation-induced amorphization resistance and radiation tolerance in structurally related oxides, Nat. Mater. 6 (3) (2007) 217–223.
[8] P. Kluth, C.S. Schnohr, O.H. Pakarinen, F. Djurabekova, D.J. Sprouster, R. Giulian, M.C. Ridgway, A.P. Byrne, C. Trautmann, D.J. Cookson, K. Nordlund, M. Toulemonde, Fine structure in swift heavy ion tracks in amorphous SiO_2, Phys. Rev. Lett. 101 (17) (2008).
[9] M.A. Subramanian, G. Aravamudan, G.V.S. Rao, Oxide pyrochlores - a review, Prog. Solid State Chem. 15 (2) (1983) 55–143.
[10] R.C. Ewing, W.J. Weber, J. Lian, Nuclear waste disposal-pyrochlore ($A_2B_2O_7$): nuclear waste form for the immobilization of plutonium and "minor" actinides, J. Appl. Phys. 95 (2004) 5949–5971.
[11] K.E. Sickafus, L. Minervini, R.W. Grimes, J.A. Valdez, M. Ishimaru, F. Li, K.J. McClellan, T. Hartmann, Radiation tolerance of complex oxides, Science 289 (5480) (2000) 748–751.
[12] L. Minervini, R.W. Grimes, K.E. Sickafus, Disorder in pyrochlore oxides, J. Am. Ceram. Soc. 83 (8) (2000) 1873–1878.
[13] B.J. Wuensch, K.W. Eberman, C. Heremans, E.M. Ku, P. Onnerud, E.M.E. Yeo, S.M. Haile, J.K. Stalick, J.D. Jorgensen, Connection between oxygen-ion conductivity of pyrochlore fuel-cell materials and structural change with composition and temperature, Solid State Ionics 129 (1–4) (2000) 111–133.
[14] F.X. Zhang, M. Lang, Z. Liu, R.C. Ewing, Pressure-induced disordering and anomalous lattice expansion in $La_2Zr_2O_7$ pyrochlore, Phys. Rev. Lett. 105 (1) (2010).
[15] F.X. Zhang, J.W. Wang, J. Lian, M.K. Lang, U. Becker, R.C. Ewing, Phase stability and pressure dependence of defect formation in $Gd_2Ti_2O_7$ and $Gd_2Zr_2O_7$ pyrochlores, Phys. Rev. Lett. 100 (2008).
[16] B.C. Chakoumakos, Systematics of the pyrochlore structure type, ideal $A_2B_2X_6Y$, J. Solid State Chem. 53 (1) (1984) 120–129.
[17] J. Lian, J. Chen, L.M. Wang, R.C. Ewing, J.M. Farmer, L.A. Boatner, K.B. Helean, Radiation-induced amorphization of rare-earth titanate pyrochlores, Phys. Rev. B 68 (2003) 134107.
[18] J. Lian, K.B. Helean, B.J. Kennedy, L.M. Wang, A. Navrotsky, R.C. Ewing, Effect of structure and thermodynamic stability on the response of lanthanide stannate-pyrochlores to ion beam irradiation, J. Phys. Chem. B 110 (5) (2006) 2343–2350.
[19] M. Lang, J. Lian, J. Zhang, F. Zhang, W.J. Weber, C. Trautmann, R.C. Ewing, Single-ion tracks in $Gd_2Zr_{2-x}Ti_xO_7$ pyrochlores irradiated with swift heavy ions, Phys. Rev. B 79 (22) (2009).
[20] M. Lang, F. Zhang, J. Zhang, J. Wang, J. Lian, W.J. Weber, B. Schuster, C. Trautmann, R. Neumann, R.C. Ewing, Review of $A_2B_2O_7$ pyrochlore response to irradiation and pressure, Nucl. Instrum. Methods Phys. Res. Sect. B-Beam Interact. Mater. Atoms 268 (2010) 2951–2959.
[21] G. Sattonnay, S. Moll, L. Thome, C. Decorse, C. Legros, P. Simon, J. Jagielski, I. Jozwik, I. Monnet, Phase transformations induced by high electronic excitation in ion-irradiated $Gd_2(Zr_xTi_{1-x})_2O_7$ pyrochlores, J. Appl. Phys. 108 (2010) 103512.
[22] C. Jiang, C.R. Stanek, K.E. Sickafus, B.P. Uberuaga, First-principles prediction of disordering tendencies in pyrochlore oxides, Phys. Rev. B 79 (10) (2009).
[23] M. Lang, M. Toulemonde, J. Zhang, F. Zhang, C.L. Tracy, J. Lian, Z. Wang, W.J. Weber, D. Severin, M. Bender, C. Trautmann, R.C. Ewing, Swift heavy ion track formation in $Gd_2Zr_{2-x}Ti_xO_7$ pyrochlore: effect of electronic energy loss, Nucl. Instrum. Methods Phys. Res. Sect. B-Beam Interact. Mater. Atoms 336 (2014) 102–115.
[24] J. Zhang, M. Lang, J. Lian, J. Liu, C. Trautmann, S. Della-Negra, M. Toulemonde, R.C. Ewing, Liquid-like phase formation in $Gd_2Zr_2O_7$ by extremely ionizing irradiation, J. Appl. Phys. 105 (11) (2009).
[25] J. Zhang, M. Lang, R.C. Ewing, R. Devanathan, W.J. Weber, M. Toulemonde,

Nanoscale phase transitions under extreme conditions within an ion track, J. Mater. Res. 25 (7) (2010) 1344–1351.
[26] J. Shamblin, C.L. Tracy, R.C. Ewing, F. Zhang, W. Li, C. Trautmann, M. Lang, Structural response of titanate pyrochlores to swift heavy ion irradiation, Acta Mater. 117 (2016) 207–215.
[27] S. Moll, G. Sattonnay, L. Thome, J. Jagielski, C. Legros, I. Monnet, Swift heavy ion irradiation of pyrochlore oxides: electronic energy loss threshold for latent track formation, Nucl. Instrum. Methods Phys. Res. Sect. B-Beam Interact. Mater. Atoms 268 (19) (2010) 2933–2936.
[28] G. Sattonnay, S. Moll, L. Thome, C. Legros, A. Calvo, M. Herbst-Ghysel, C. Decorse, I. Monnet, Effect of composition on the behavior of pyrochlores irradiated with swift heavy ions, Nucl. Instrum. Methods Phys. Res. Sect. B-Beam Interact. Mater. Atoms 272 (2012) 261–265.
[29] J. Zhang, M. Toulemonde, M. Lang, J.M. Costantini, S. Della-Negra, R.C. Ewing, C60 and U ion irradiation of $Gd_2Ti_xZr_{2-x}O_7$ pyrochlore, J. Mater. Res. 30 (2015) 2456–2466.
[30] W. Panero, L. Stixrude, R. Ewing, First-principles calculation of defect-formation energies in the $Y_2(Ti,Sn,Zr)_2O_7$ pyrochlore, Phys. Rev. B 70 (2004) 54110.
[31] M. Sanjuán, C. Guglieri, S. Díaz-Moreno, G. Aquilanti, A. Fuentes, L. Olivi, J. Chaboy, Raman and x-ray absorption spectroscopy study of the phase evolution induced by mechanical milling and thermal treatments in $R_2Ti_2O_7$ pyrochlores, Phys. Rev. B 84 (2011) 1–18.
[32] P.E.R. Blanchard, R. Clements, B.J. Kennedy, C.D. Ling, E. Reynolds, M. Avdeev, A.P.J. Stampfl, Z.M. Zhang, L.Y. Jang, Does local disorder occur in the pyrochlore zirconates? Inorg. Chem. 51 (24) (2012) 13237–13244.
[33] P.E.R. Blanchard, S. Liu, B.J. Kennedy, C.D. Ling, M. Avdeev, J.B. Aitken, B.C.C. Cowie, A. Tadich, Investigating the local structure of lanthanoid hafnates Ln(2)Hf(2)O(7) via diffraction and spectroscopy, J. Phys. Chem. C 117 (5) (2013) 2266–2273.
[34] S.T. Norberg, S. Hull, S.G. Eriksson, I. Ahmed, F. Kinyanjui, J.J. Biendicho, Pyrochlore to fluorite transition: the $Y_2(Ti_{1-x}Zr_x)_2O_7$ ($0.0 \leq x \leq 1.0$) system, Chem. Mater. 24 (2012) 4294–4300.
[35] G. King, C.M. Thompson, J.E. Greedan, A. Llobet, Local structure of the vacancy disordered fluorite Yb_3TaO_7 from neutron total scattering, J. Mater. Chem. A 1 (35) (2013) 10487–10494.
[36] J. Shamblin, M. Feygenson, J. Neuefeind, C.L. Tracy, F. Zhang, S. Finkeldei, D. Bosbach, H. Zhou, R.C. Ewing, M. Lang, Probing disorder in isometric pyrochlore and related complex oxides, Nat. Mater 15 (5) (2016) 507–511.
[37] L. Cai, J.C. Nino, Complex ceramic structures. I. Weberites, Acta Crystallogr. Sect. B-Struct. Sci. 65 (2009) 269–290.
[38] J.M. Solomon, J. Shamblin, M. Lang, A. Navrotsky, M. Asta, Chemical ordering in substituted fluorite oxides: a computational investigation of $Ho_2Zr_2O_7$ and $RE_2Th_2O_7$ (RE=Ho, Y, Gd, Nd, La), Sci. Rep. 6 (2016).
[39] C.L. Tracy, J. Shamblin, S. Park, F. Zhang, C. Trautmann, M. Lang, R.C. Ewing, Role of composition, bond covalency, and short-range order in the disordering of stannate pyrochlores by swift heavy ion irradiation, Phys. Rev. B 94 (6) (2016) 064102.
[40] R. Sachan, V.R. Cooper, B. Liu, D.S. Aidhy, B.K. Voas, M. Lang, X. Ou, C. Trautmann, Y. Zhang, M.F. Chisholm, W.J. Weber, Forging fast ion conducting nanochannels with swift heavy ions: the correlated role of local electronic and atomic structure, J. Phys. Chem. C 121 (1) (2017) 975–981.
[41] J.F. Ziegler, M.D. Ziegler, J.P. Biersack, SRIM - the stopping and range of ions in matter (2010), Nucl. Instrum. Methods Phys. Res. Sect. B-Beam Interact. Mater. Atoms 268 (11–12) (2010) 1818–1823.
[42] J. Neuefeind, M. Feygenson, J. Carruth, R. Hoffmann, K.K. Chipley, The Nanoscale ordered MAterials diffractometer NOMAD at the spallation neutron Source SNS, Nucl. Instrum. Methods Phys. Res. Sect. B-Beam Interact. Mater. Atoms 287 (2012) 68–75.
[43] C.L. Farrow, P. Juhas, J.W. Liu, D. Bryndin, E.S. Bozin, J. Bloch, T. Proffen, S.J.L. Billinge, PDFfit2 and PDFgui: computer programs for studying nanostructure in crystals, J. Physics-Condensed Matter 19 (33) (2007).
[44] N.J. Hess, B.D. Begg, S.D. Conradson, D.E. McCready, P.L. Gassman, W.J. Weber, Spectroscopic investigations of the structural phase transition in $Gd_2(Ti_{1-y}Zr_y)_2O_7$ pyrochlores, J. Phys. Chem. B 106 (2002) 4663–4677.
[45] Y. Li, P.M. Kowalski, G. Beridze, A.R. Birnie, S. Finkeldei, D. Bosbach, Defect formation energies in $A_2B_2O_7$ pyrochlores, Scr. Mater. 107 (2015) 18–21.
[46] S. Finkeldei, P. Kegler, P.M. Kowalski, C. Schreinemachers, F. Brandt, A.A. Bukaemskiy, V.L. Vinograd, G. Beridze, A. Shelyug, A. Navrotsky, D. Bosbach, Composition dependent order-disorder transition in $Nd_xZr_{1-x}O_{2-0.5x}$ pyrochlores: a combined structural, calorimetric and ab initio modeling study, Acta Mater. 125 (2017) 166–176.
[47] H.Y. Xiao, W.J. Weber, Y. Zhang, X.T. Zu, S. Li, Electronic excitation induced amorphization in titanate pyrochlores: an ab initio molecular dynamics study, Sci. Rep. 5 (2015).